ORIGINAL PAPER

Characterization of Acid and Basic Sites on Zirconia Surfaces and Nanoparticles by Adsorbed Probe Molecules: A Theoretical Study

Farahnaz Maleki[1] · Gianfranco Pacchioni[1] [ID]

Abstract

Acid and basic sites on monoclinic and tetragonal zirconia were investigated at the DFT level by computing IR and NMR properties of adsorbed probe molecules. Regular and stepped ZrO_2 surfaces as well as stoichiometric zirconia nanoparticles have been considered. Acidity and basicity were probed by the adsorption of carbon monoxide and pyrrole, respectively. CO adsorption shows a positive shift of the C–O stretching frequency in IR spectra while the C atom of CO is shielded and ^{13}C chemical shifts moves to higher field as a function of the strength of the acid site. For the study of basic sites we used a pyrrole molecule, but the interaction between the pyrrole ring and the surface leads to adsorption modes that cannot be used to titrate the surface basicity. On the other hand, at high coverage the molecule assumes an upright position and the formation of a hydrogen bond of the pyrrole NH group with the oxygen atoms of the surfaces provides a proxy of the basic properties of these sites. In particular, we focus on changes of the N–H IR frequency, ^{1}H, ^{15}N, and ^{17}O NMR chemical shifts and their correlations with the surface basicity. Among the correlations found, that between the N–H stretching frequency of adsorbed pyrrole and the ^{17}O NMR chemical shift of the O ion where the molecule is bound show a nice linear correlation. These two properties can provide useful information about the basic character of various O sites on the surface of zirconia.

Graphic Abstract
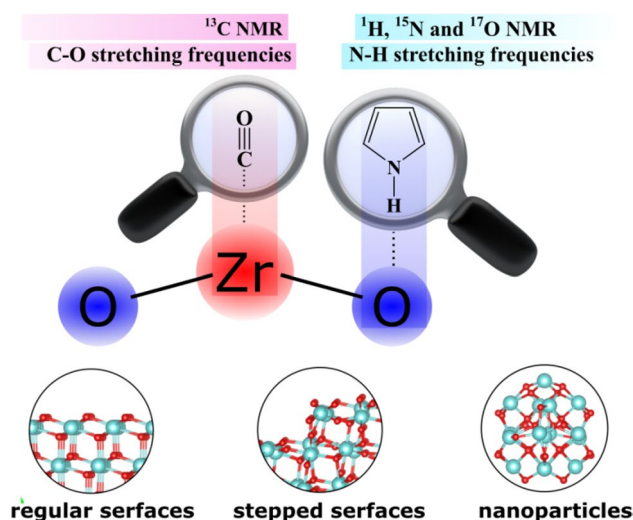
Keywords Oxide surfaces · Acid–base properties · Monoclinic and tetragonal zirconia · CO and pyrrole adsorption · Density functional theory

Extended author information available on the last page of the article

1 Introduction

Identifying the acid and basic strength of surface sites is essential to rationalize the catalytic properties of oxide surfaces. Metal cations are potential electron charge acceptors, i.e. Lewis acids, while O^{2-} anions play the role of conjugated bases [1, 2]. The selectivity of many reactions is influenced not only by the nature of the acidic and basic sites but also by their number and acid/base strength.

Zirconium dioxide (ZrO_2) is an important material with acid/base character [3] and is very stable under oxidizing and reducing atmospheres [4]. For this reason, is an interesting catalyst support [5] and a catalyst on its own [6]. Zirconia has at least five stable structural polymorphs [7, 8] with different properties. The monoclinic ZrO_2 phase (m-ZrO_2) is stable at low temperature [9]. Around 1400 and 2600 K, there is a first- and second-order phase transition to tetragonal [10] and cubic [11] structures, respectively. The most stable facet of tetragonal zirconia (t-ZrO_2), (101), is the same as the most stable cubic zirconia (111) surface [12]. The brookite (orthorhombic-I) and cotunnite (orthorhombic-II) phases are high pressure-induced phases of zirconia [7, 13].

We have chosen t-ZrO_2 (101) and m-ZrO_2 ($\bar{1}$11) surfaces for this study since these are the most stable surfaces of the two common phases of zirconia [14]. On the other hand, nanocrystalline materials exhibit unique structural features with distinct properties and catalytic activity [15]. In this work we focus on fully dehydrated models of different zirconia structures. This is because our interest is on the Lewis acidity and basicity of the surface, while the presence of surface OH groups can result also in Broensted acidity.

Carbon monoxide (CO) has been widely studied as a probe molecule to characterize the Lewis acidity of zirconia [16, 17] using infrared (IR) spectroscopy [16, 18]. Other studies, such as temperature-programmed desorption [19], and calorimetry [20], as well as theoretical studies [21, 22] have been reported. The determination of surface basicity is more complex as the probe molecules, such as carbon dioxide (CO_2) [23], may dissociate or give rise to complex surface reactions. Adsorption of pyrrole (C_4NH_5) as a probe molecule to detect the basic sites on the surface of metal oxides and to estimate their basic strength has been studied by IR [24, 25] and nuclear magnetic resonance (NMR) [26–28] spectroscopies, and will be considered here from a theoretical point of view.

Studies of the acid–base properties of tetragonal [21, 29] and monoclinic [30] ZrO_2 as well as of other metal oxides [31, 32] have been reported already. Structural defects of oxide surfaces such as steps, exhibiting low-coordinated O^{2-} and M^{n+} sites, are expected to affect the interaction with adsorbates [33]. However, not always the change in coordination number results in a measurable change in acidity or basicity [21].

In this work we will discuss the acidity and basicity of regular t-ZrO_2 (101) and m-ZrO_2 ($\bar{1}$11) and stepped t-ZrO_2 (134) and m-ZrO_2 ($\bar{2}$12) surfaces, as well as of zirconia nanoparticles of size ranging between 1.5 and 2 nm, $(ZrO_{2\pm x})_n$ with n = 13–85 [34–38].

2 Methods

The calculations have been performed by means of the VASP 5.4.4 package [39–41]. The valence electrons, H (1s), C (2s, 2p), N (2s, 2p), O (2s, 2p) and Zr (4s, 5s, 4p, 4d), are expanded on a set of plane waves with a kinetic cut-off of 400 eV, whereas the core electrons are treated with the Projector Augmented Wave (PAW) approach [42, 43]. The generalized gradient approximation (GGA) for the exchange–correlation functional was applied, with the Perdew−Burke−Ernzerhof (PBE) formulation [44]. The GGA+U approach implemented by Dudarev et al. was used to partly correct the self-interaction error of GGA functionals, that affects the electronic structure [45, 46]. In particular, the onsite Coulomb correction, $U_{eff} = U–J$, was set to 4 eV for the 4d states of Zr atoms [34, 47]. The D3 dispersion energy was included by means of the Becke−Johnson damping [48, 49].

The lattice parameters of bulk m- and t-zirconia were fully optimized with a kinetic energy cutoff of 600 eV and an $8 \times 8 \times 8$ Monkhorst−Pack k-point grid; the resulting parameters were fixed in all slab calculations. A slab of four and five ZrO_2 layers was used for the ($\bar{1}$11) and (101) surfaces. For the ($\bar{1}$11) surface, a 2×2 supercell ($Zr_{64}O_{128}$) was used, whereas for the (101) surface, a 3×2 supercell with $Zr_{60}O_{120}$ formula was taken. For the stepped surfaces, on the basis of the previous work [50], we adopted 1×1 supercells of t-ZrO_2 (134) surface with 3 layers of ZrO_2 ($Zr_{24}O_{48}$). The monoclinic stepped surface ($\bar{2}$12) [5, 51] were modeled with a three-layer thick stepped zirconia film with a 2×1 unit cell and $Zr_{60}O_{120}$ formula. For all cases, a vacuum region > 10 Å is present to remove the slab−slab interactions. For zirconia nanostructures, the stoichiometric nanoparticles $Zr_{16}O_{32}$ and $Zr_{40}O_{80}$ were considered [34, 35].

For all models, we performed structural relaxations of all atoms with convergence criteria of 10^{-5} eV and 10^{-2} eV/Å for the electronic and ionic loops, respectively. The sampling of the reciprocal space is set to the Γ-point for m-ZrO_2 ($\bar{1}$11) and ($\bar{2}$12), t-ZrO_2 (101) and zirconia nanoparticles: this choice still ensures reasonable accuracy, given the large size of the adopted supercells. For t-ZrO_2 (134) stepped surface, we used $3 \times 2 \times 1$ k-point meshes.

The isotropic chemical shift (δ_{iso}) is computed as $\delta_{iso} = \sigma_{ref} - \sigma_{calc}$, where σ_{ref} is the shielding value of the reference and σ_{calc} is the chemical shielding obtained in VASP. For ^{1}H, ^{15}N, and ^{13}C NMR, on the basis of experimental reports, we consider tetramethylsilane (TMS) [52], ammonia (NH$_3$) [53], and TMS [54], respectively, as the references with 31, 255 and 178 ppm chemical shielding calculated by VASP. For ^{17}O NMR, on the basis of previous reports considering that the bulk oxygen anions have more regular arrangements than the oxygen anions at the surface, a constant value can be used to determine the reference chemical shift (δ_{ref}):

$$\delta_{ref} = \delta_{iso}(bulk(exp)) - m\sigma_{calc}(bulk(calc)) \tag{1}$$

here $\delta_{iso}(bulk(exp))$ is the experimental chemical shift of bulk m-ZrO$_2$ (325 ppm) [55]. $\sigma_{calc}(bulk(calc))$ refers to the chemical shielding of oxygen atoms in inner layers that have constant value (-344 ppm for regular m-ZrO$_2$ ($\bar{1}$11) slab); m is a gradient assumed to be equal -1 [55]. Thus, δ_{ref} can be determined as -17 ppm for m-ZrO$_2$ surfaces. The results of ^{17}O NMR chemical shift (δ_{iso}) of the m-ZrO$_2$ surfaces are summarized in the Supporting Information. For t-ZrO$_2$ surfaces and nanoparticles, we employed the same strategy of our previous work to calculate δ_{ref} which is fixed at -36 ppm [38]. Since the reference for calculation of the ^{17}O chemical shift of oxygen anions in m- and t-ZrO$_2$ slabs is different, we consider the chemical shielding of water [55], 317 ppm, as the reference for calculation of ^{17}O chemical shift of O atoms in the CO adsorbed molecule.

Vibrational frequencies are calculated within the harmonic approximation via diagonalization of the dynamical matrix. The active fragment for the ionic displacements is restricted to the adsorbed molecules and the surface ions directly taking part in the adsorption process.

Finally, the adsorption energies (E_{ADS}) have been calculated according to the following equation:

$$E_{ADS} = E(x/ZrO_2) - E(x)(g) - E(ZrO_2) \tag{2}$$

where x is the adsorbed molecule and ZrO$_2$ the oxide support.

3 Results and Discussions

3.1 Acid Properties: CO Adsorption

In this section, we explore the acidity of Zr atoms in different ZrO$_2$ structures. Changes of stretching frequency and ^{13}C and ^{17}O NMR of adsorbed CO in comparison with the free CO molecule will be discussed.

3.1.1 Regular m-ZrO$_2$ ($\bar{1}$11) and t-ZrO$_2$ (101) Surfaces

On the m-ZrO$_2$ ($\bar{1}$11) surface there are four non-equivalent Zr atoms, Fig. 1. Zr-A, Zr-B, and Zr-C are six-fold coordinated, Zr$_{6c}$, while Zr-D is seven-fold coordinated, Zr$_{7c}$. Figure 2a–c shows the CO adsorption on Zr-A to -C, respectively. The properties of CO adsorption on all zirconia surfaces are summarized in Table 1. During the optimization, starting from CO on Zr-D, CO moves to Zr-A. The adsorption energies (E_{ADS}) of CO to the Zr atoms are in the range -0.49 to -0.56 eV, Table 1. The CO frequencies are blue-shifted with respect to the free CO, from a minimum of $+12$ to a maximum of $+29$ cm^{-1}. Experimentally, shifts of $+31/+51$ cm^{-1} have been reported for CO on m-ZrO$_2$ [56]. The C–O bond length decreases slightly by adsorption on both m- and t-ZrO$_2$ surfaces. The Zr-C bond distances are in the range 2.506–2.576 Å. The bonding of CO to the surface does not imply a charge transfer, as it is shown by the net CO Bader charges that are always smaller than 0.03 |e| in absolute value (see Table S1).

The results of ^{13}C NMR show that the C atom of adsorbed CO is shielded, and $\delta_{iso}(^{13}$C) decreases by about -9 ppm and

Fig. 1 Position of Zr atoms (big blue spheres: A-D) and O atoms (small red spheres: 1–8) on the first layer of the m-ZrO$_2$ ($\bar{1}$11) surface. **a** Side, **b** Top views
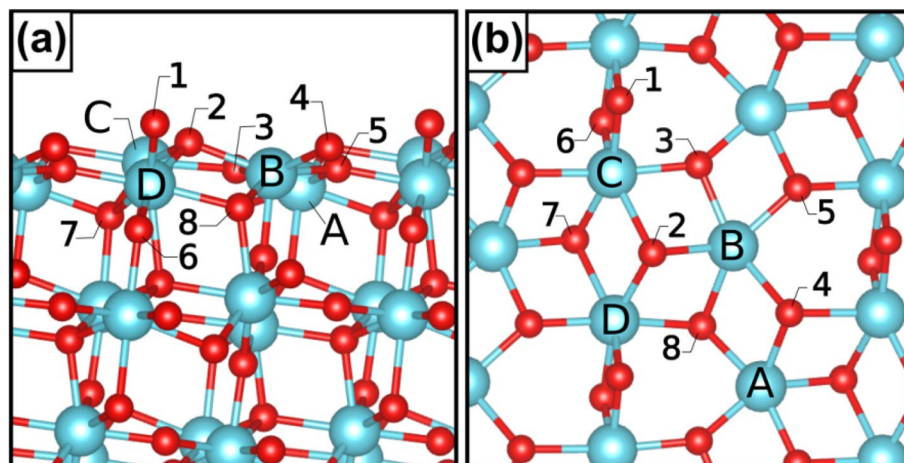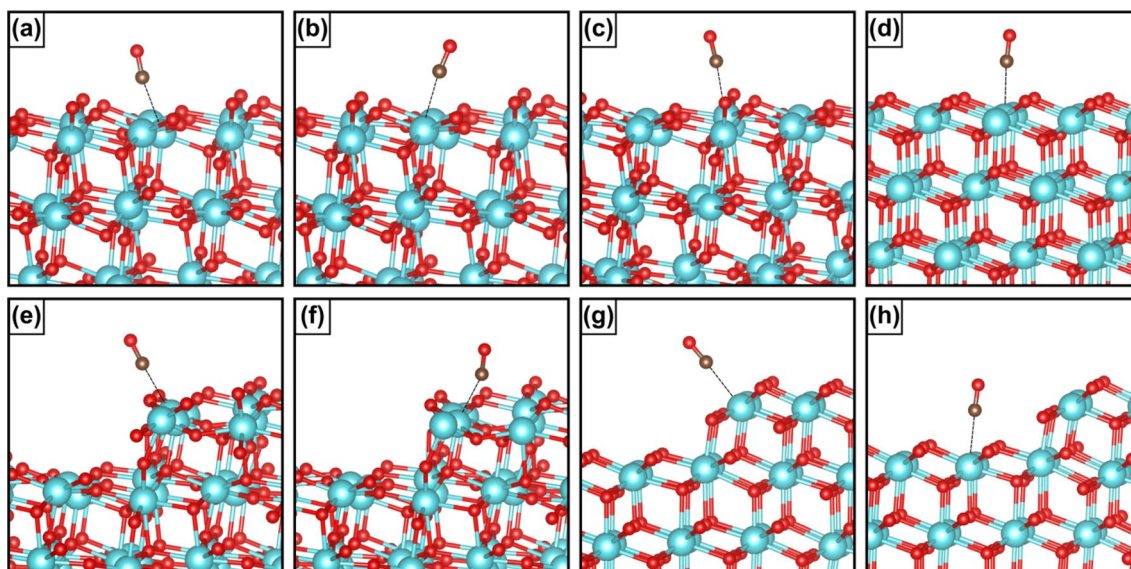
Fig. 2 Optimal structures of CO on regular, **a–d**, and stepped, **e–h**, ZrO$_2$ surfaces. The panels **a** to **c**, **e** and **f** show the adsorption on m-ZrO$_2$ surfaces and the panels **d**, **g** and **h** the adsorption on t-ZrO$_2$ surfaces. Blue, red and brown spheres are Zr, O and C atoms, respectively

Table 1 Adsorption energy (E_{ADS}, eV), bond length (R, Å), C–O stretching frequency (ν, cm^{-1}) and ^{13}C chemical shift (δ_{iso}, ppm) of CO on ZrO$_2$ surfaces and Zr$_{16}$O$_{32}$ and Zr$_{40}$O$_{80}$ nanoparticles

	Figs.	Site	E_{ADS}	R_{CO}	R_{Zr-C}	ν_{CO}	$\Delta\nu_{CO}$	$\delta_{iso}(^{13}C)$	$\Delta\delta_{iso}(^{13}C)$
m-ZrO$_2$ ($\bar{1}$11)	2 (a)	Zr$_{6c}$A	− 0.56	1.142	2.576	2136	13	192	− 10
	2 (b)	Zr$_{6c}$B	− 0.55	1.140	2.571	2152	29	193	− 9
	2 (c)	Zr$_{6c}$C	− 0.49	1.142	2.549	2135	12	193	− 9
t-ZrO$_2$ (101)	2 (d)	Zr$_{7c}$	− 0.50	1.142	2.506	2130	7	200	− 2
m-ZrO$_2$ ($\bar{2}$12)	2 (e)	Zr$_{5c}$	− 0.54	1.140	2.553	2149	26	193	− 9
	2 (f)	Zr$_{6c}$	− 0.52	1.142	2.638	2129	6	194	− 8
t-ZrO$_2$ (134)	2 (g)	Zr$_{6c}$	− 0.61	1.139	2.553	2159	36	199	− 3
	2 (h)	Zr$_{7c}$	− 0.39	1.143	2.570	2119	− 4	201	− 1
Zr$_{16}$O$_{32}$	4 (a)	Zr$_{4c}$	− 0.85	1.144	2.515	2070	− 53	49	− 153
	4 (b)	Zr$_{5c}$	− 0.68	1.144	2.458	2114	− 9	209	7
	4 (c)	Zr$_{5c}$	− 0.66	1.137	2.564	2175	52	195	− 7
	4 (d)	Zr$_{5c}$	− 0.65	1.138	2.582	2168	45	193	− 9
Zr$_{40}$O$_{80}$	4 (e)	Zr$_{6c}$	− 0.70	1.137	2.505	2183	60	194	− 8
	4 (f)	Zr$_{6c}$	− 0.64	1.140	2.528	2155	32	197	− 5
	4 (g)	Zr$_{6c}$	− 0.62	1.140	2.503	2152	29	197	− 5
	4 (h)	Zr$_{5c}$	− 0.50	1.140	2.556	2146	23	197	− 5

The bond length of free CO molecule is 1.144 Å

goes to higher field. The changes of ^{17}O chemical shift of the O atom of CO are not significant, and will not be further discussed.

On the t-ZrO$_2$ (101) surface there is only one kind of zirconium, the 7-coordinated zirconium cation (Zr$_{7c}$), Fig. 2d. The interaction of CO with Zr$_{7c}$ has an adsorption energy of − 0.50 eV, close to that computed for Zr$_{6c}$ sites on the m-ZrO$_2$ ($\bar{1}$11) surface, see Table 1. The C–O stretching frequency and $\delta_{iso}(^{13}C)$ are shifted by + 7 cm^{-1}

and − 2 ppm, respectively. The experimental data for changes in C–O stretching frequency on t-ZrO$_2$ surface is reported + 51 cm^{-1} [18]. The difference with respect to our calculations is due to the fact that higher levels of theory (hybrid functionals) and correction for anharmonic effects need to be included in order to obtain a quantitative estimate of this property. On the other hand, the trend is correct and the CO stretching frequency can be safely used to probe different acid sites on the surface of zirconia.

3.1.2 Stepped m-ZrO$_2$ ($\bar{2}$12) and t-ZrO$_2$ (134) Surfaces

In this section we explore the adsorption of CO on low-coordinated Zr sites on stepped m-ZrO$_2$ ($\bar{2}$12), Fig. 2e, f, and t-ZrO$_2$ (134), Fig. 2g, surfaces. The maximum and minimum adsorption energies of CO, -0.61 and -0.39 eV, are observed for Zr$_{6c}$ and Zr$_{7c}$ on stepped (Fig. 2g) and regular terrace (Fig. 2h) sites of the t-ZrO$_2$ (134) surface, respectively. Also, the shift in stretching frequency of CO on the stepped site of t-ZrO$_2$ (134) is the largest observed $+36$ cm^{-1} (to be compared to a shift of -4 cm^{-1} on the flat region of the step). The bond distance of C to Zr is between 2.506 and 2.638 Å.
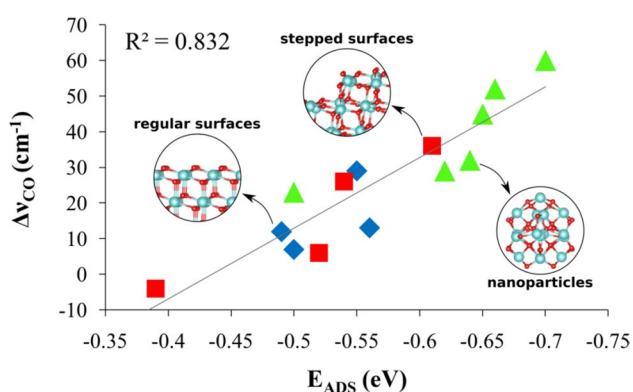

Fig. 3 The plot of E$_{ADS}$ against $\Delta\nu_{CO}$ of the CO molecule on the regular and the stepped surfaces (Fig. 2a–h) and nanostructures (Fig. 4c–h) of ZrO$_2$

In Fig. 3 we plot the change in CO stretching frequency versus the adsorption energy, E$_{ADS}$, for all zirconia structures considered.

On Table 1 we have reported the ^{13}C chemical shifts (δ_{iso}) of adsorbed CO. Upon adsorption, δ_{iso}(^{13}C) of CO is shifted to lower ppm (-1 to -3 ppm for tetragonal and -8 to -10 ppm for monoclinic surfaces) while the changes of ^{17}O NMR of adsorbed CO are not noticeable. These shifts appear too small to provide a measure of the different properties of the various acid sites.

3.1.3 ZrO$_2$ Nanoparticles

Now we consider two zirconia stoichiometric clusters to model the properties of zirconia nanostructures. Details on how these have been obtained and on their electronic structure can be found in refs [34–37]. We have studied the adsorption of CO on different surface Zr atoms of Zr$_{16}$O$_{32}$ (Fig. 4a–d) and Zr$_{40}$O$_{80}$ (Fig. 4e–h). The adsorption energy of CO is in the range -0.50 to -0.85 eV, i.e. it is a bit stronger than on the regular surface. The CO bond distances, with two exceptions, are slightly shortened with respect to the free molecule (1.144 Å), an effect that results in a positive shift in CO vibrational frequency of $+23$ to $+60$ cm^{-1}, see Table 1. However, two CO adsorption modes on Zr$_{16}$O$_{32}$, Fig. 4a and b, show red-shifts in the C–O stretching frequency by -53 and -9 cm^{-1}, respectively. This is a clear indication that some Zr ions on the ZrO$_2$ nanoparticles still have residual electron density to be back-donated to the 2π* MO of the adsorbed CO molecule. For the same reason, also,
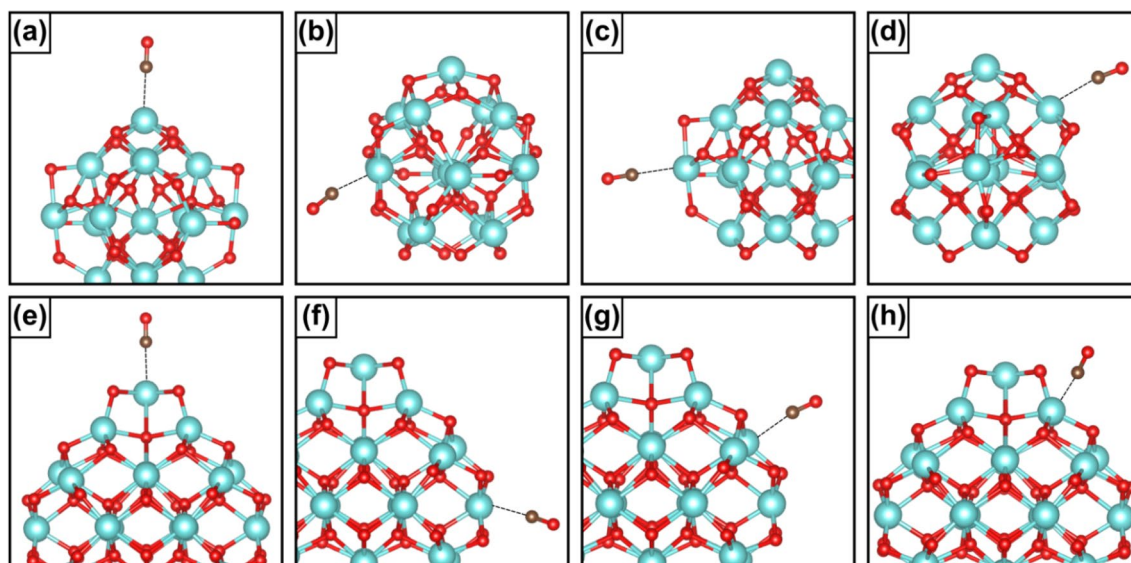

Fig. 4 Optimal structures of CO on Zr$_{16}$O$_{32}$ (**a–d**) and Zr$_{40}$O$_{80}$ (**e–h**) nanoparticles. The blue, red and brown spheres are Zr, O and C atoms, respectively

the changes in $\delta_{iso}(^{13}C)$ are out of range compared to the other sites (Fig. 4c–h), see Table 1. This shows that some specific Zr sites in the stoichiometric nanoparticles have much weaker acid character than other sites. The bonding of CO to the apical Zr site of $Zr_{16}O_{32}$, Fig. 4a, shows a CO frequency shift and a NMR signal completely different from the other sites. This is clear manifestation of the fact that we are in a non-scalable regime, where properties change with size but also with the site considered. Here, a partial accumulation of charge on the apical Zr atom results in an enhanced back donation to CO which reinforces the bond with the nanoparticle. The presence of such sites is not observed in zirconia particles of larger size.

The changes in $\delta_{iso}(^{13}C)$ of adsorbed CO on $Zr_{16}O_{32}$ and $Zr_{40}O_{80}$ nanoparticles, Fig. 4c–h and Table 1, are in a range from -5 to -9 ppm while the changes of ^{17}O NMR are, once more, negligible.

The adsorption energy of the CO molecule on various Zr cations of different surfaces (Fig. 2a–h) and nanostructures (Fig. 4c–h) has been plotted against the CO stretching frequency (Fig. 3). The resulting curve shows some correlation of the two properties ($R^2 = 0.83$), and can be taken as a descriptor of the acid character of the sites. In particular, higher CO frequency shifts are found in correspondence of Zr ions of the nanoparticles where the coordination is lower.

3.2 Basic Properties: Pyrrole Adsorption

To measure the Lewis basic properties of zirconia we have considered the adsorption of a pyrrole molecule. This molecule has been selected after having tried other potential molecular probes, such as CO_2, $CHCl_3$, SO_2, BF_3, and acetonitrile, but all these molecules tend to react with the zirconia surface, with bond breaking that prevents from a direct comparison of the various adsorption sites. Two types of interaction can be observed for pyrrole: one where the ring interacts with the metal cations in a flat orientation, dominated by dispersion forces, and a second one where the bonding occurs via formation of a hydrogen bond between the NH group of the pyrrole molecule and an oxygen ion of the surface. Both interactions have been observed in zeolites, and it has been reported that a large shift to lower frequencies of the NH vibration upon adsorption is almost entirely due to the formation of a hydrogen bond [57]. Figure 5a and b show the pyrrole ring interaction with the regular t-ZrO_2 (101) and m-ZrO_2 ($\bar{1}11$) surfaces, respectively, with adsorption energies of -0.66 eV and -0.81 eV, respectively.

On zirconia, at zero coverage, the flat bonding mode (ring interaction) is preferred compared to the formation of a hydrogen bond. However, things are different when more molecules are adsorbed in the supercell, modeling high coverage. Considering two co-adsorbed pyrrole molecules, Fig. 5c and d, the flat bonding mode is still preferred; however, with three co-adsorbed molecules Fig. 5e

Fig. 5 Optimized structures of a pyrrole molecule interacting nearly parallel to the surface with **a** t-ZrO_2 (101) and **b** m-ZrO_2($\bar{1}11$) surfaces and high coverage adsorption **c–e** on t-ZrO_2 (101) surface. The blue, red, brown, gray and white spheres are Zr, O, C, N and H atoms, respectively. Distances in Angstrom
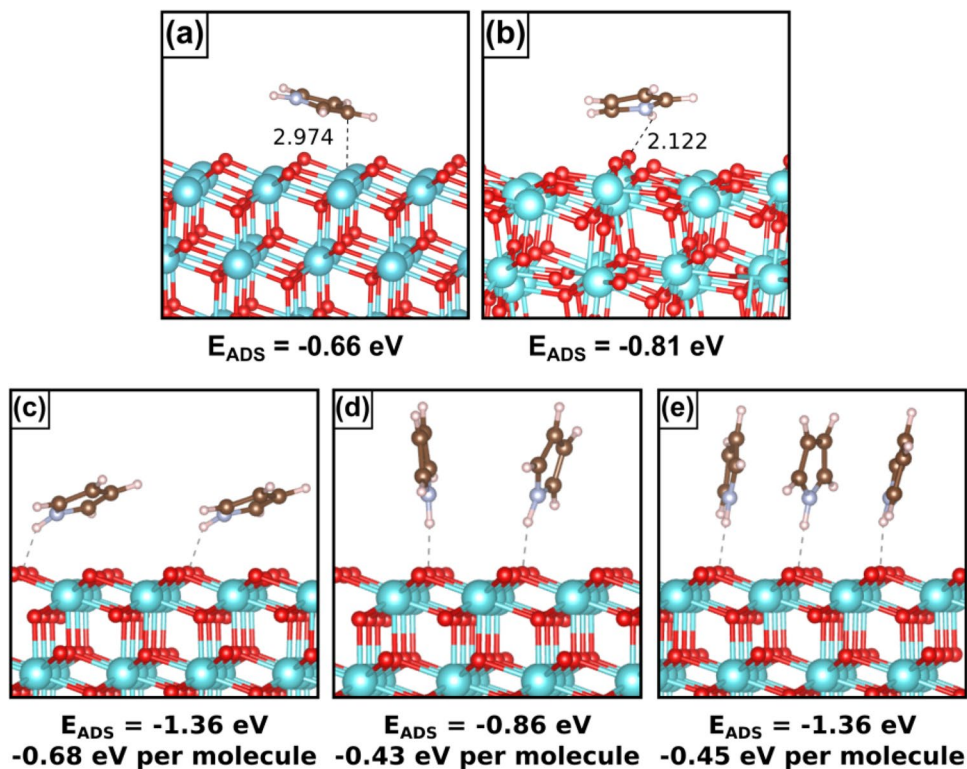
only the normal mode is stable due to steric effects. Thus, although adsorbed pyrrole molecules at low coverage prefer to stay parallel to the surface, Fig. 5a–c, at high coverage the upright adsorption mode is dominant Fig. 5e. We have considered the pyrrole bonded to the surface via the NH group as a probe molecule to explore the basicity of different oxygen atoms on the surface, Fig. 6. The data refer to the isolated pyrrole molecule, but since the intermolecular interactions are weak, the results are not expected to change as a function of coverage.

3.2.1 Regular m-ZrO$_2$ ($\bar{1}$11) and t-ZrO$_2$ (101) Surfaces

There are 8 different oxygen atoms on the surface of m-ZrO$_2$ ($\bar{1}$11), Fig. 1: O1 to O5 are on the surface while O6 to O8 are in the sub-surface, and cannot bind the pyrrole molecule. O1 is two coordinated (O$_{2c}$) while the other oxygen anions (O2-O4) are O$_{3c}$.

The adsorption energies (E$_{ADS}$) of the pyrrole bound via NH group to the surface O atoms go from -0.42 to -0.49 eV, see Table 2. These values are slightly smaller in absolute value than for the flat adsorption mode, Fig. 5. The distances of the H atom from the surface O ion are

between 1.766 and 1.883 Å. Due to this interaction, the NH bond length slightly increases compared to the gas phase (1.013 Å) and the N–H stretching frequencies are significantly red-shifted by -189 to -380 cm^{-1}, Table 2. This points to a different strength of the basic O sites on the surface. Thus, while the adsorption energies do not show a strong site-dependence, the N–H vibrational frequency does.

In Fig. 7 we have plotted the O$_{surf}$-H$_{NH}$ bond distance, measuring the distance of the NH group of the pyrrole molecule from the surface, against the N–H vibrational frequency, potentially an observable quantity. The results show an almost linear correlation (R^2 = 0.88) for the four O adsorption sites of the m-ZrO$_2$ and t-ZrO$_2$ surfaces. In particular, when the molecule goes closer to the surface, the NH stretching frequency exhibits a larger red-shift. This points to a more pronounced basic character of the O sites where this occurs. The bonding of pyrrole to the surface does not imply a charge transfer, as it is shown by the Bader charges. The charge on pyrrole due to the interaction with the surface is always smaller than 0.03 |e| in absolute value (Table S2).

Now we discuss the chemical shifts. ^{1}H chemical shifts have been used to study the basicity of various sites in zeolites using pyrrole adsorption [26–28]. In these studies ^{1}H
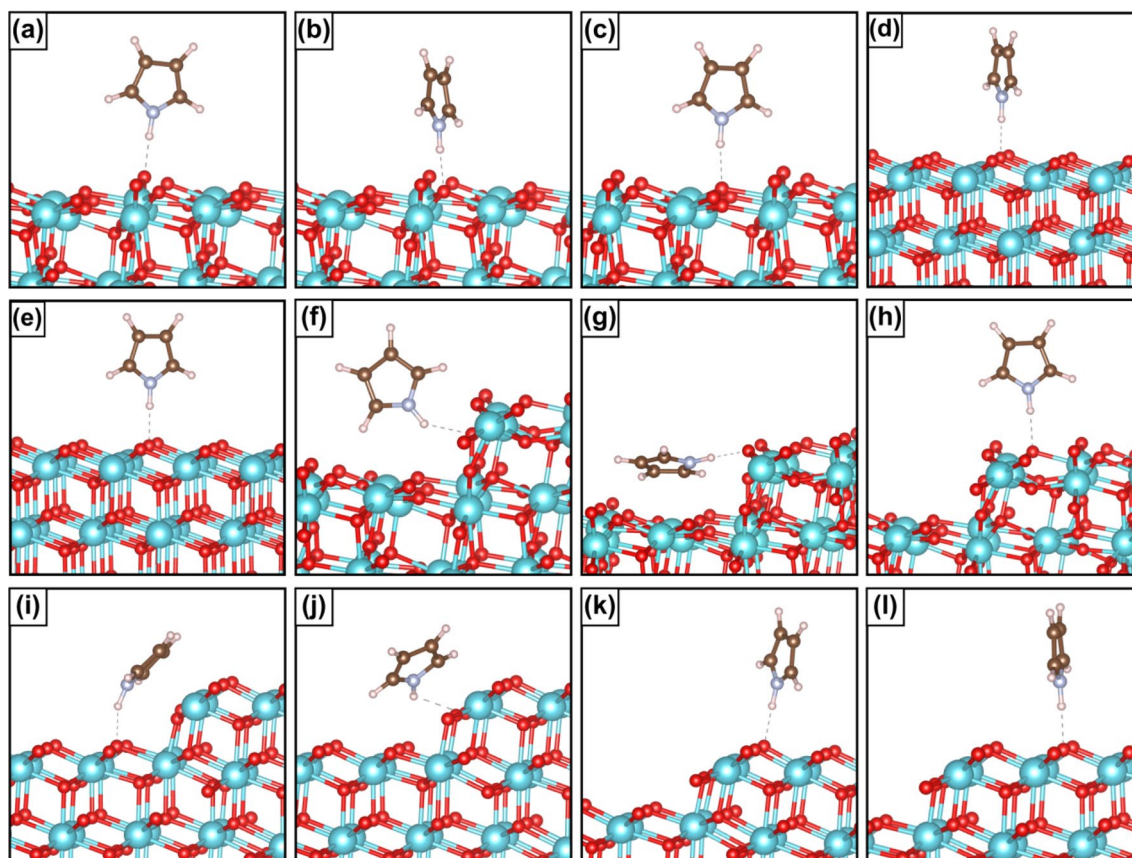

Fig. 6 Optimal structures of pyrrole bound via NH to O ions on the regular (**a–e**) and the stepped (**f–l**) zirconia surfaces. **a–c** and **f–h**: m-ZrO$_2$; **d**, **e** and **i** to **l** t-ZrO$_2$. The blue, red, brown, gray and white spheres are Zr, O, C, N and H atoms, respectively

Table 2 Adsorption energy (E_{ADS}, eV), bond lengths (R, Å), N–H stretching frequencies (ν, cm^{-1}), and ^{1}H, ^{15}N and ^{17}O NMR chemical shift (δ_{iso}, ppm) of pyrrole on ZrO$_2$ surfaces and Zr$_{16}$O$_{32}$ and Zr$_{40}$O$_{80}$ nanoparticles

	Figs.	Site	E_{ADS}	R_{NH}	R_{OH}	ν_{NH}	$\Delta\nu_{NH}$	δ_{iso} (^{1}H)	$\Delta\delta_{iso}$ (^{1}H)	δ_{iso} (^{15}N)	$\Delta\delta_{iso}$ (^{15}N)	δ_{iso} (^{17}O$_{surf}$)	δ_{iso} (^{17}O$_{ad}$)	$\Delta\delta_{iso}$ (^{17}O)
m-ZrO$_2$ ($\bar{1}$11)	6 (a)	O$_{2c}$(O1)	−0.49	1.033	1.766	3218	−380	16	7	201	27	591	532	−59
	6 (b)	O$_{3c}$ (O2)	−0.45	1.023	1.883	3409	−189	14	5	196	22	422	401	−21
	6 (c)	O$_{3c}$ (O4)	−0.44	1.026	1.843	3325	−273	14	5	196	22	422	394	−28
t-ZrO$_2$ (101)	6 (d)	O$_{3c}$	−0.42	1.030	1.806	3256	−342	15	6	195	21	454	411	−43
	6 (e)	O$_{3c}$	−0.42	1.030	1.807	3260	−338	15	6	195	21	454	411	−43
m-ZrO$_2$ ($\bar{2}$12)	6 (f)	O$_{3c}$	−0.58	1.021	2.046	3454	−144	14	5	196	22	428	414	−14
	6 (g)	O$_{2c}$	−1.08	1.041	1.755	3257	−341	17	8	214	40	527	471	−56
	6 (h)	O$_{3c}$	−0.31	1.026	1.887	3335	−263	15	6	194	20	428	390	−38
t-ZrO$_2$ (134)	6 (i)	O$_{3c}$	−1.26	1.050	1.781	2976	−622	15	6	212	38	440	416	−24
	6 (j)	O$_{3c}$	−1.15	1.027	2.126	3377	−221	13	4	207	33	440	478	38
	6 (k)	O$_{3c}$	−0.42	1.028	1.841	3288	−310	14	5	193	19	440	398	−42
	6 (l)	O$_{3c}$	−0.47	1.029	1.820	3280	−318	15	6	195	21	440	392	−48
Zr$_{16}$O$_{32}$	13 (a)	O$_{2c}$	−0.49	1.043	1.721	3041	−557	15	6	204	30	556	477	−79
	13 (b)	O$_{2c}$	−0.35	1.033	1.793	3213	−385	13	4	195	21	639	568	−71
	13 (c)	O$_{2c}$	−0.30	1.031	1.839	3248	−350	13	4	194	20	464	421	−43
Zr$_{40}$O$_{80}$	13 (d)	O$_{2c}$	−0.44	1.035	1.782	3190	−408	14	5	198	24	576	514	−62
	13 (e)	O$_{3c}$	−0.36	1.024	1.874	3370	−228	12	3	190	16	436	407	−29
	13 (f)	O$_{2c}$	−0.35	1.028	1.822	3302	−296	14	5	193	19	584	530	−54
	13 (g)	O$_{3c}$	−0.32	1.027	1.853	3317	−281	13	4	191	17	403	372	−31

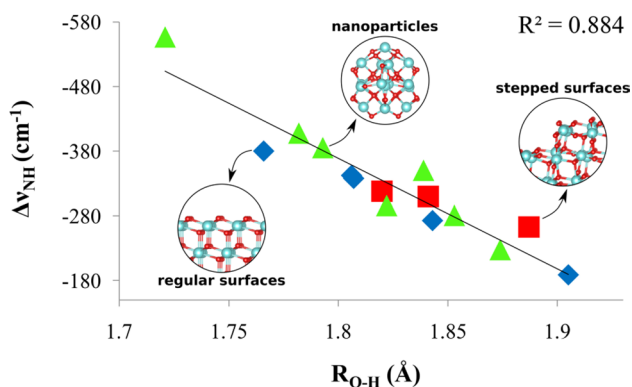The bond length of N–H bond in free pyrrole molecule is 1.013 Å

Fig. 7 Correlation between the shift in N–H stretching frequency, $\Delta\nu_{NH}$, and the distance of the pyrrole molecule from the O ion of the zirconia surface, R_{O-H}
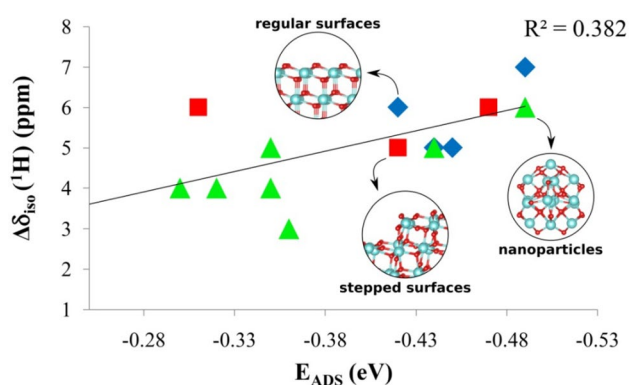

Fig. 8 Correlation between the changes in ^{1}H NMR chemical shift and the adsorption energy of the pyrrole molecule on various ZrO$_2$ structures

chemical shifts of 9–11 ppm have been measured (slightly shifted with respect to the free molecule which has a value of 7.1 ppm), and a linear correlation with the proton affinity with the ^{1}H chemical shift has been shown based on DFT calculations [26]. Here instead of the absolute value of the ^{1}HN chemical shifts, δ_{iso}(^{1}H), we discuss the change compared to the free molecule due to the adsorption on a basic site, $\Delta\delta_{iso}$(^{1}H). In our models $\Delta\delta_{iso}$(^{1}H) of adsorbed pyrrole is in the range +5/+7 ppm, Table 2. We have plotted

$\Delta\delta_{iso}$(^{1}H) against the pyrrole adsorption energy in Fig. 8. On the regular surfaces no clear trend emerges, due to the rather close values of both δ_{iso}(^{1}H) and E_{ADS}. However, as it will be discussed below, a general although not regular tendency towards an increase of $\Delta\delta_{iso}$(^{1}H) for stronger surface-pyrrole bonds if found when all the other zirconia structures are considered, Fig. 8.

We consider now the changes in ^{15}N NMR chemical shifts. Due to the low natural abundance of the ^{15}N nucleus

this is not easily accessible experimentally, although some examples have been reported in the literature [58]. As for the H case, also here we refer to the changes occurring on this property with respect to a free gas-phase pyrrole molecule. These changes, $\Delta\delta_{iso}(^{15}N)$, for the regular surfaces go from $+21$ to $+27$ ppm, Table 2. If one plots these values for the five adsorption sites on the regular m-ZrO_2 and t-ZrO_2 surfaces versus the adsorption energy, an almost linear correlation is found, Fig. 9 ($R^2 = 0.92$). In particular, an increase of the adsorption energy corresponds to an increase of the $\Delta\delta_{iso}(^{15}N)$. However, if we include into this plot also the results of pyrrole adsorption on the stepped surfaces and on the nanoparticles (see below) the correlation becomes much worse and no simple trend can be established. We attribute this to the very different interaction of pyrrole on the regular surfaces and on the low-coordinated sites.

Recently, we have reported the measurement of the basicity of alkaline-earth oxide surfaces by means of ^{17}O NMR calculations [59]. We found that the ^{17}O NMR signal of the O ion directly bound to a probe molecule shifts considerably compared to the clean surface [59]. The average ^{17}O NMR chemical shifts for the O atoms on the clean zirconia surfaces before and after adsorption of pyrrole are given in Table 2.

In Fig. 10 we have plotted the distance of the H atom of pyrrole from the surface, R_{O-H}, versus $\Delta\delta_{iso}(^{17}O)$. The plot shows a clear correlation of the two quantities, with stronger negative shifts of $\Delta\delta_{iso}(^{17}O)$ in correspondence of shorter O–H distances (see squares in Fig. 10).

The O ions involved in the bonding with pyrrole are shielded, and $\delta_{iso}(^{17}O)$ decreases from -21 to -59 ppm with respect to $\delta_{iso}^{avg}(^{17}O)$ of the clean surfaces, see Table 2. Plotting $\Delta\delta_{iso}(^{17}O)$ versus the change in N–H vibrational frequency, $\Delta\nu_{NH}$, we found a nearly linear correlation, see Table 2 and Fig. 11. This confirms that the ^{17}O NMR signal of the O ion where a species is adsorbed can provide interesting information about the nature of the basic site, as found
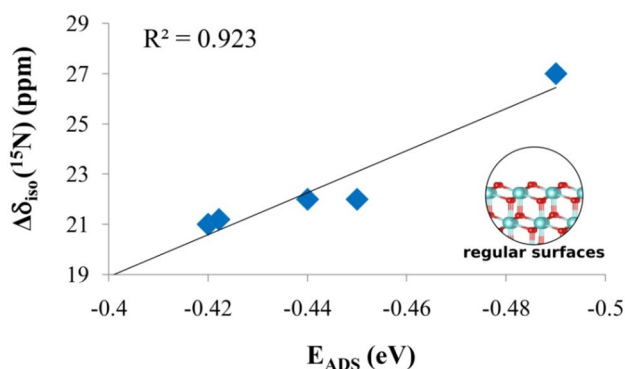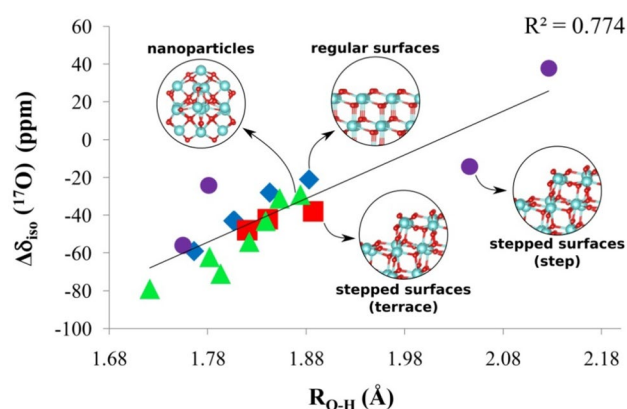

Fig. 10 Correlation between the changes in ^{17}O NMR chemical shift and the distance of pyrrole from the surface, R_{O-H}, for various ZrO_2 surfaces and nanoparticles

for the alkaline-earth oxides [59]. The full set of values of the ^{17}O NMR chemical shifts is reported in the Supporting Information.

3.2.2 Stepped m-ZrO_2 ($\bar{2}12$) and t-ZrO_2 (134) Surfaces

Next, we consider pyrrole adsorption on both terrace and stepped O sites of m-ZrO_2 ($\bar{2}12$) and t-ZrO_2 (134) surfaces, Fig. 6 and Table 2. On the flat areas of the stepped surfaces the adsorption energies of pyrrole do not show significant changes with respect to the regular surface; the proximity of the step has practically no effect, due to the local character of the bond. Figure 6f shows the simultaneous formation of two hydrogen bonds of the pyrrole NH group with two O atoms; here the adsorption energy becomes -0.58 eV. This stronger interaction does not correspond to a more pronounced variation of the N–H bond distance (elongated
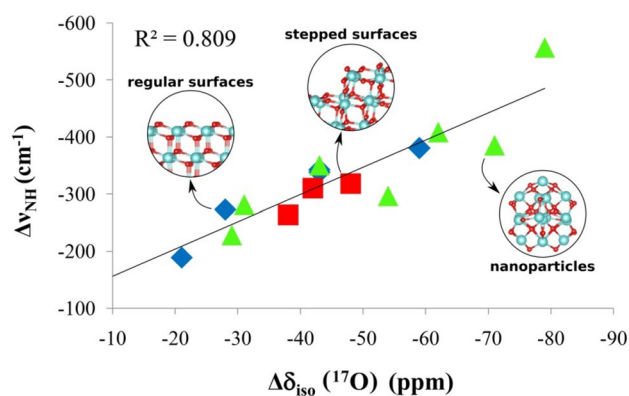

Fig. 9 Correlation between the changes in ^{15}N NMR chemical shift and the adsorption energy of the pyrrole molecule on the regular sites of m-ZrO_2 and t-ZrO_2 surfaces

Fig. 11 Correlation between the shift in N–H stretching frequency of the pyrrole molecule and the changes in ^{17}O NMR chemical shift for pyrrole adsorbed on O ions of the regular and stepped m-ZrO_2 and t-ZrO_2 surfaces and on zirconia nanoparticles

by 0.008 Å only with respect to the free molecule) and N–H stretching frequency (red-shifted by − 144 cm^{-1} with respect to gas-phase).

The adsorption of pyrrole on the steps of m-ZrO$_2$ ($\bar{2}$12), Fig. 6g, and t-ZrO$_2$ (134), Fig. 6i and j, show a different bonding mode. In these cases, in addition to the formation of a hydrogen bond of the pyrrole NH group, the pyrrole ring interacts via dispersion forces with the surface. This is similar to the bonding mode found for pyrrole in the cavity of zeolites containing trapped metal ions [57]. In these structures the bond strength increases considerably (− 1.08 eV for m-ZrO$_2$ ($\bar{2}$12) and − 1.26 and − 1.15 eV for t-ZrO$_2$ (134)), due to the multiple interaction mode. As found for zeolites [57], also here the changes of NH frequency are noticeable. $\Delta\nu_{NH}$ on the stepped sites of m-ZrO$_2$ ($\bar{2}$12), Fig. 6g, and t-ZrO$_2$ (134), Fig. 6i and j is red-shifted by − 341, − 622 and − 221 cm^{-1}, respectively. These values are not included in the correlation of Fig. 11 where the NH stretching frequencies are plotted versus the ^{17}O chemical shift as the bonding mode is different.

The results of the ^{1}H NMR show that in all structures the H atom of the NH group is deshielded by adsorption on the O ions of the surface, i.e. δ_{iso} goes to the lower fields. The maximum $\Delta\delta_{iso}(^1H)$ is for pyrrole on O$_{2c}$ sites of regular, Fig. 6a, and stepped m-ZrO$_2$ surfaces, Fig. 6f, + 7 and + 8 ppm, respectively. $\Delta\delta_{iso}(^1H)$ for various O$_{3c}$ sites is + 5/+ 6 ppm, see Table 2. The $\Delta\delta_{iso}(^1H)$ values for pyrrole adsorbed on the stepped surfaces have been included in Fig. 8. No clear trend emerges if one takes only these values, as similar chemical shifts of 5–6 ppm, correspond to adsorption energies from 0.3 to 0.5 eV.

More relevant is $\delta_{iso}(^{15}N)$ NMR as this has shown a linear correlation with E$_{ADS}$ for adsorption on the regular zirconia surfaces, Fig. 9. On the models of the stepped surfaces, if we consider the flat regions, Fig. 6h, k, l, $\delta_{iso}(^{15}N)$ assumes similar values, + 19/+ 27 ppm, as on the regular surfaces. More pronounced are $\Delta\delta_{iso}(^{15}N)$ for the adsorption on the stepped sites, Fig. 6g, i and j + 40, + 38 and + 33 ppm, respectively. However, we did not include these data in the plot of Fig. 9 because of the different bonding mode.

The results of ^{17}O NMR chemical shifts, Table 2, show that the surface O ions interacting with pyrrole are shielded, and $\delta_{iso}(^{17}O)$ decreases by − 14/− 56 ppm with respect to the $\delta_{iso}^{avg}(^{17}O)$ of the clean surfaces. However, for other structures, Fig. 6j, the O ion on the step interacting with NH is deshielded, and δ_{iso} increases by + 38, respectively, see also Fig. 10. This is due to the fact that pyrrole interacts with the surface via ring bonding mode, and the H-bonding becomes very long, 2.126 Å, Table 2.

The values of $\delta_{iso}(^{17}O)$ for the stepped surfaces have been plotted against the N–H stretching frequency, Fig. 11, and the points are behaving as found for the regular surfaces, showing an overall linear trend. This reinforces the

idea that $\delta_{iso}(^{17}O)$ can be used to measure the basicity of sites where pyrrole binds via NH forming a hydrogen bond.

3.2.3 ZrO$_2$ Nanoparticles

Here we consider pyrrole adsorption on the Zr$_{16}$O$_{32}$ and Zr$_{40}$O$_{80}$ nanoparticles. The interaction via the aromatic ring bound to Zr cations is clearly preferred, with adsorption energies of − 1.27 to − 1.70 eV Fig. 12.

This is much stronger than the formation of a hydrogen bond between the NH group of the pyrrole molecule and the O atoms of the nanoparticle (in the range − 0.32 to − 0.49 eV, Table 2 and Fig. 13a–g). So, one can rule out the possibility to experimentally test the basicity of the O$_{2c}$ or O$_{3c}$ surface ions by using pyrrole as a probe molecule. In some calculations we have been able to find a minimum structure for the H-bonded complex via NH group, with formation of a metastable complex. In other cases, however, the molecule does not bind via H but spontaneously binds in a flat mode. In this respect, the following discussion is purely hypothetical and the properties of the adsorbed pyrrole molecule, Table 2, represent an internal test of the different nature of the surface O atoms. For instance, the N–H stretching frequencies for the adsorbed molecules have been plotted against the distance of pyrrole from the surface of the nanoparticle, R$_{O-H}$, Fig. 7, showing the same trend found for the other O sites of the flat and stepped zirconia surfaces.

We also computed $\Delta\delta_{iso}(^1H)$, $\Delta\delta_{iso}(^{15}N)$ and $\Delta\delta_{iso}(^{17}O)$ NMR chemical shifts (see also Supplementary Information), and we reported these values in the corresponding curves. They will be discussed in the concluding section.
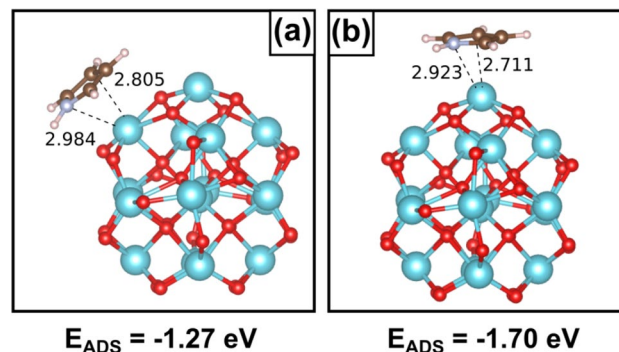

Fig. 12 The interaction of pyrrole ring with Zr$_{16}$O$_{32}$ nanoparticle. The blue, red, brown, gray and white spheres are Zr, O, C, N and H atoms, respectively. Distances in Angstrom
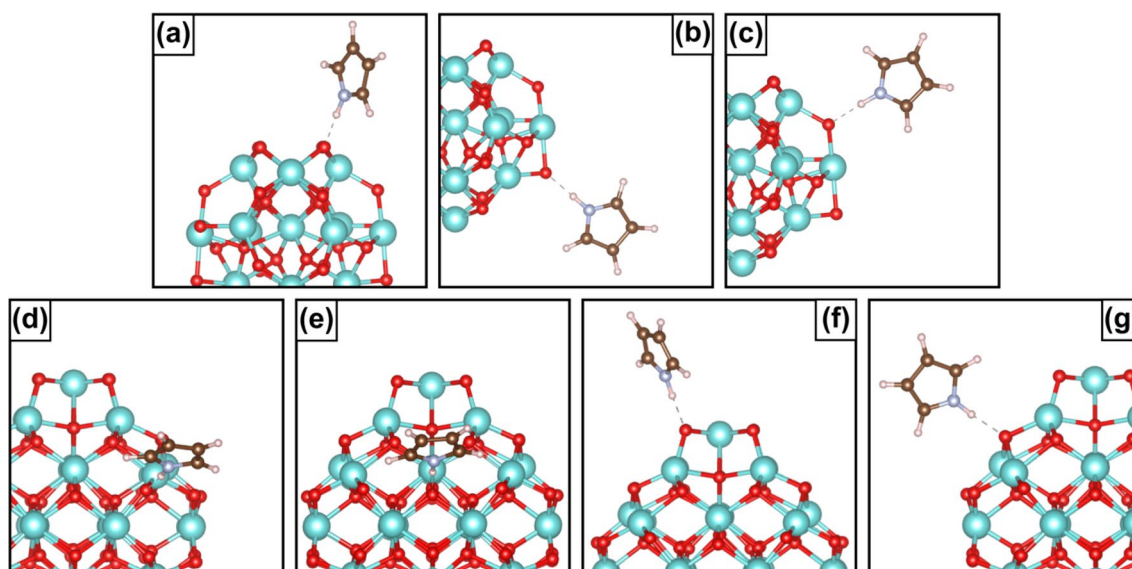
Fig. 13 Optimal structures of hydrogen bonded pyrrole via NH group with the O atoms of the surface of $Zr_{16}O_{32}$ (**a–c**) and $Zr_{40}O_{80}$ (**d–g**) nanostructures. The blue, red, brown, gray and white spheres are Zr, O, C, N and H atoms, respectively

4 Conclusions

In this work we have investigated the acid and base sites on monoclinic and tetragonal zirconia using DFT derived IR and NMR properties of adsorbed probe molecules. To this end, regular and stepped surfaces of m- and t-ZrO_2 as well as stoichiometric zirconia nanoparticles have been considered. Acidity and basicity were probed by the adsorption of CO and pyrrole molecules, respectively. The average adsorption energy of CO on the different sites of regular and stepped m- and t-ZrO_2 surfaces is about -0.52 eV, and increases slightly for nanoparticles (-0.66 eV). The adsorption energy of CO shows a correlation with the C–O stretching frequency. In particular, the blue-shift of the CO stretching mode, indicating a stronger Zr acid site, increases moving from the regular surfaces to the stepped surfaces and the nanoparticles. This confirms the potential use of CO as a probe to measure the acidic character of cation sites on the surface of zirconia.

The results of NMR calculations show that the C atom of adsorbed CO is shielded and $\delta_{iso}(^{13}C)$ goes to the higher field, but the shifts are very small and no direct correlation with the surface acidity can be established.

Pyrrole has been used to monitor the surface basicity [26–28]. In zeolites this has been used as a probe molecule to titrate the basic character of O ions of the cages [57]. Pyrrole can interact with oxide surfaces in two different bonding modes, with the center of the ring close to a cation or with the NH group pointing to a surface anion. Only this second bonding mode is of some interest for the study of surface basicity. Unfortunately, for all ZrO_2 structures considered, the ring interaction, dominated by polarization and dispersion forces, is stronger. Bonding via the NH group become preferred at high coverage, due to steric effects, which allows a theoretical study of the properties.

A series of correlations have been studied that can be useful for the identification of the strength of the basic sites. An almost linear correlation with good regression coefficient, $R^2 = 0.88$, is found between the NH vibrational frequency and the distance of the pyrrole molecule from the O ion of the surface, R_{O-H}, Fig. 7. On the contrary, no correlation exists with the strength of the adsorption energy. Similar correlations have been analyzed for the NMR chemical shifts.

The ^1H signal of the proton in contact with the surface shows a general trend, with more positive shifts corresponding to stronger adsorption energies of the pyrrole molecule, Fig. 8. However, the data points for the various structures considered are rather scattered, and this cannot be taken as a robust descriptor of the strength of the basic site.

A higher correlation is found for the ^{15}N chemical shift, in particular if we plot this versus the pyrrole adsorption energy on the O sites on the regular m-ZrO_2 and t-ZrO_2 surfaces, Fig. 9. Here the regression is very good, with $R^2 = 0.92$. If we consider all the structures studied, we still find a linear trend, even including some structures where the pyrrole molecule is not only bound via H-bonding, see Fig. S4.

We recently showed that the ^{17}O NMR chemical shift can provide in principle useful information about the basic character of surface sites in alkaline-earth oxides [59]. Here we confirm this potential role. In fact, while no direct correlation exists between $\delta_{iso}(^{17}O)$ NMR of the O ion directly

bound to the pyrrole molecule and the adsorption energy, an almost linear correlation if found when we plot this quantity versus the distance of the molecule from the surface, R_{O-H}, Fig. 10. The R^2 value is not particularly high, 0.78, but this also partly due to the flat nature of the potential energy surface, which results in some uncertainty on the computed O–H distances.

Finally, a good correlation is found between the two key quantities that can be used to titrate the basic character of the surface using pyrrole adsorption: the N–H stretching frequency and the ^{17}O NMR chemical shift, Fig. 11. The two quantities show a nice linear correlation despite the very irregular nature of some of the structures considered. This confirms that these two properties can provide in principles useful information about the basic character of various O sites on the surface of zirconia.

Compliance with Ethical Standards

Conflict of interest The authors declare no conflict of interest.

Research Involving Human and Animal Rights This research does not involve experiments on Animals or Humans.

References

1. Knöuzinger H (1976) Specific poisoning and characterization of catalytically active oxide surfaces. Adv Catal 25:184–271
2. Corma A (1995) Inorganic solid acids and their use in acid-catalyzed hydrocarbon reactions. Chem Rev 95(3):559–614
3. Tanabe K, Yamaguchi T (1994) Acid-base bifunctional catalysis by ZrO₂ and its mixed oxides. Catal Today 20(2):185–197
4. Yamaguchi T (1994) Application of ZrO₂ as a catalyst and a catalyst support. Catal Today 20(2):199–217
5. Wang C-M, Fan K-N, Liu Z-P (2007) Origin of oxide sensitivity in gold-based catalysts: a first principle study of CO oxidation over Au supported on monoclinic and tetragonal ZrO₂. J Am Chem Soc 129(9):2642–2647
6. Audry F, Hoggan P, Saussey J, Lavalley J, Lauron-Pernot H, Le Govic A (1997) Infrared study and quantum calculations of the conversion of methylbutynol into hydroxymethylbutanone on zirconia. J Catal 168(2):471–481
7. Leger JM, Tomaszewski P, Atouf A, Pereira AS (1993) Pressure-induced structural phase transitions in zirconia under high pressure. Phys Rev B 47(21):14075
8. Kisi EH, Howard C (1998) Crystal structures of zirconia phases and their inter-relation. Key Eng Mater 153–154:1–36
9. Howard C, Hill R, Reichert B (1988) Structures of ZrO₂ polymorphs at room temperature by high-resolution neutron powder diffraction. Acta Crystallogr B 44(2):116–120
10. Teufer G (1962) The crystal structure of tetragonal ZrO₂. Acta Crystallogr 15(11):1187–1187
11. Yoshimura M (1988) Phase stability of zirconia. Am Ceram Soc Bull 67(12):1950–1955
12. Hofmann A, Clark SJ, Oppel M, Hahndorf I (2002) Hydrogen adsorption on the tetragonal ZrO₂ (101) surface: a theoretical study of an important catalytic reactant. Phys Chem Chem Phys 4(14):3500–3508
13. Liu L-G (1980) New high pressure phases of ZrO₂ and HfO₂. J Phys Chem Solids 41(4):331–334
14. Christensen A, Carter EA (1998) First-principles study of the surfaces of zirconia. Phys Rev B 58(12):8050
15. Henglein A (1989) Small-particle research: physicochemical properties of extremely small colloidal metal and semiconductor particles. Chem Rev 89(8):1861–1873
16. Kouva S, Honkala K, Lefferts L, Kanervo J (2015) Monoclinic zirconia, its surface sites and their interaction with carbon monoxide. Catal Sci Technol 5(7):3473–3490
17. Morierra C, Aschieri R, Volante M (1988) Surface characterization of zirconium oxide I. Surface activation and the development of a strong Lewis acidity. Mater Chem Phys 20(6):539–557
18. Bolis V, Morterra C, Fubini B, Ugliengo P, Garrone E (1993) Temkin-type model for the description of induced heterogeneity: CO adsorption on group 4 transition metal dioxides. Langmuir 9(6):1521–1528
19. He M-Y, Ekerdt JG (1984) Temperature-programmed studies of the adsorption of synthesis gas on zirconium dioxide. J Catal 87(1):238–254
20. Ushakov SV, Navrotsky A (2005) Direct measurements of water adsorption enthalpy on hafnia and zirconia. Appl Phys Lett 87(16):164103
21. Chen H-YT, Tosoni S, Pacchioni G (2016) A DFT study of the acid–base properties of anatase TiO₂ and tetragonal ZrO₂ by adsorption of CO and CO₂ probe molecules. Surf Sci 652:163–171
22. Korhonen ST, Calatayud M, Krause AOI (2008) Structure and stability of formates and carbonates on monoclinic zirconia: a combined study by density functional theory and infrared spectroscopy. J Phys Chem C 112(41):16096–16102
23. Köck E-M, Kogler M, Bielz T, Klötzer B, Penner S (2013) In situ FT-IR spectroscopic study of CO₂ and CO adsorption on Y₂O₃, ZrO₂, and yttria-stabilized ZrO₂. J Phys Chem C 117(34):17666–17673
24. Scokart PO, Rouxhet PG (1980) Characterization of the basicity of oxides through the infrared study of pyrrole adsorption. J Chem Soc Faraday Trans 1(76):1476–1489

25. Binet C, Jadi A, Lamotte J, Lavalley J (1996) Use of pyrrole as an IR spectroscopic molecular probe in a surface basicity study of metal oxides. J Chem Soc Faraday Trans 92(1):123–129

26. Yi X, Li G, Huang L, Chu Y, Liu Z, Xia H, Zheng A, Deng F (2017) An NMR scale for measuring the base strength of solid catalysts with pyrrole probe: a combined solid-state NMR experiment and theoretical calculation study. J Phys Chem C 121(7):3887–3895

27. Wang Y, Han XW, Ji A, Shi L, Hayashi S (2005) Basicity of potassium-salt modified hydrotalcite studied by ^{1}H MAS NMR using pyrrole as a probe molecule. Microporous Mesoporous Mater 77(2–3):139–145

28. Sánchez-Sánchez M, Blasco T (2000) Pyrrole as an NMR probe molecule to characterise zeolite basicity. Chem Comm 6:491–492

29. Bolis V, Magnacca G, Cerrato G, Morterra C (2002) Effect of sulfation on the acid-base properties of tetragonal zirconia. A calorimetric and IR spectroscopic study. Top Catal 19(3–4):259–269

30. Cerrato G, Bordiga S, Barbera S, Morterra C (1997) A surface study of monoclinic zirconia (m-ZrO_2). Surf Sci 377:50–55

31. Tanabe K (1989) New solid acids and bases: their catalytic properties. Stud Surf Sci Catal 51:142–159

32. Tanaka K-I, Ozaki A (1967) Acid-base properties and catalytic activity of solid surfaces. J Catal 8(1):1–7

33. Pacchioni G, Ricart JM, Illas F (1994) Ab initio cluster model calculations on the chemisorption of CO2 and SO2 probe molecules on MgO and CaO (100) surfaces. A theoretical measure of oxide basicity. J Am Chem Soc 116(22):10152–10158

34. Puigdollers AR, Illas F, Pacchioni G (2016) Structure and properties of zirconia nanoparticles from density functional theory calculations. J Phys Chem C 120(8):4392–4402

35. Ruiz Puigdollers A, Tosoni S, Pacchioni G (2016) Turning a nonreducible into a reducible oxide via nanostructuring: opposite behavior of bulk ZrO_2 and ZrO_2 nanoparticles toward H_2 adsorption. J Phys Chem C 120(28):15329–15337

36. Puigdollers AR, Illas F, Pacchioni G (2017) ZrO_2 nanoparticles: a density functional theory study of structure, properties and reactivity. Rend Lincei-Sci Fis 28(1):19–27

37. Albanese E, Ruiz Puigdollers A, Pacchioni G (2018) Theory of ferromagnetism in reduced ZrO_{2-x} nanoparticles. ACS omega 3(5):5301–5307

38. Maleki F, Pacchioni G (2019) DFT study of ^{17}O NMR spectroscopy applied to zirconia surfaces and nanoparticles. J Phys Chem C 123(35):21629–21638

39. Kresse G, Furthmüller J (1996) Efficiency of ab-initio total energy calculations for metals and semiconductors using a plane-wave basis set. Comp Mater Sci 6(1):15–50

40. Kresse G, Hafner J (1993) Ab initio molecular dynamics for liquid metals. Phys Rev B 47(1):558

41. Kresse G, Hafner J (1994) Ab initio molecular-dynamics simulation of the liquid-metal–amorphous-semiconductor transition in germanium. Phys Rev B 49(20):14251

42. Kresse G, Joubert D (1999) From ultrasoft pseudopotentials to the projector augmented-wave method. Phys Rev B 59(3):1758

43. Blöchl PE (1994) Projector augmented-wave method. Phys Rev B 50(24):17953

44. Perdew JP, Burke K, Ernzerhof M (1996) Generalized gradient approximation made simple. Phys Rev Lett 77(18):3865

45. Anisimov VI, Zaanen J, Andersen OK (1991) Band theory and Mott insulators: Hubbard U instead of Stoner I. Phys Rev B 44(3):943

46. Dudarev S, Botton G, Savrasov S, Humphreys C, Sutton A (1998) Electron-energy-loss spectra and the structural stability of nickel oxide: an LSDA+ U study. Phys Rev B 57(3):1505

47. Livraghi S, Paganini MC, Giamello E, Di Liberto G, Tosoni S, Pacchioni G (2019) Formation of reversible adducts by adsorption of oxygen on Ce–ZrO_2: an unusual η^2 ionic superoxide. J Phys Chem C 123(44):27088–27096

48. Grimme S, Ehrlich S, Goerigk L (2011) Effect of the damping function in dispersion corrected density functional theory. J Comput Chem 32(7):1456–1465

49. Grimme S, Antony J, Ehrlich S, Krieg H (2010) A consistent and accurate ab initio parametrization of density functional dispersion correction (DFT-D) for the 94 elements H-Pu. J Chem Phys 132(15):154104

50. Tosoni S, Chen HYT, Pacchioni G (2015) A DFT study of the reactivity of anatase TiO_2 and tetragonal ZrO_2 stepped surfaces compared to the regular (101) terraces. ChemPhysChem 16(17):3642–3651

51. Kouva S, Andersin J, Honkala K, Lehtonen J, Lefferts L, Kanervo J (2014) Water and carbon oxides on monoclinic zirconia: experimental and computational insights. Phys Chem Chem Phys 16(38):20650–20664

52. Vancompernolle T, Merle N, Capet F, Del Rosal I, Laurent M, Delevoye L, Pourpoint F, Gauvin RM (2019) Grafting of a new bis-silylamido aluminum species on silica: insight from solid-state NMR into interactions with the surface. Dalton Trans 48(16):5243–5252

53. Maeda S, Mori T, Sasaki C, Kunimoto K-K, Kuwae A, Hanai K (2005) Structural investigation of microbial poly (ε-L-lysine) derivatives with azo dyes by solid-state ^{13}C and ^{15}N NMR. Polym Bull 53(4):259–267

54. Bosacek V (1993) Formation of surface-bonded methoxy groups in the sorption of methanol and methyl iodide on zeolites studied by carbon-13 MAS NMR spectroscopy. J Phys Chem 97(41):10732–10737

55. Shen L, Wu X-P, Wang Y, Wang M, Chen J, Li Y, Huo H, Hou W, Ding W, Gong X-Q, Peng L (2019) ^{17}O solid-state NMR studies of ZrO_2 nanoparticles. J Phys Chem C 123(7):4158–4167

56. Thang HV, Tosoni S, Fang L, Bruijnincx P, Pacchioni G (2018) Nature of sintering-resistant, single-atom Ru species dispersed on zirconia-based catalysts: a DFT and FTIR study of CO adsorption. ChemCatChem 10(12):2634–2645

57. Kučera J, Nachtigall P, Kotrla J, Košová G, Čejka J (2004) Pyrrole as a probe molecule for characterization of basic sites in ZSM-5: a combined FTIR spectroscopy and computational study. J Phys Chem B 108(41):16012–16022

58. Lorente P, Shenderovich IG, Golubev NS, Denisov GS, Buntkowsky G, Limbach HH (2001) ^{1}H/^{15}N NMR chemical shielding, dipolar ^{15}N, ^{2}H coupling and hydrogen bond geometry correlations in a novel series of hydrogen-bonded acid–base complexes of collidine with carboxylic acids. Magn Reson Chem 39(S1):S18–S29

59. Maleki F, Pacchioni G (2019) ^{17}O NMR as a measure of basicity of alkaline-earth oxide surfaces: a theoretical study. J Chem Phys 151(22):224705

Affiliations

Farahnaz Maleki[1] · Gianfranco Pacchioni[1]

✉ Gianfranco Pacchioni
   gianfranco.pacchioni@unimib.it

[1] Dipartimento di Scienza dei Materiali, Università di Milano-Bicocca, via R. Cozzi 55, 20125 Milano, Italy